Orbitally modulated photoexcited Si I emission in the eclipsing composite-spectrum binary ζ Aurigae

G. M. Harper,[1]★ R. E. M. Griffin,[2]★ P. D. Bennett[3]★ and N. O'Riain[4]

[1]*CASA, University of Colorado, Boulder, CO 80309-0389, USA*
[2]*Dominion Astrophysical Observatory, Victoria, BC V9E 2E7, Canada*
[3]*Saint Mary's University, Halifax, Nova Scotia, NS B3H 3C3, Canada*
[4]*School of Physics, Trinity College, Dublin 2, Ireland*

ABSTRACT

We examine the little-known phenomenon of orbitally modulated Si I emission at $\lambda\,3905.523$ Å and $\lambda\,4102.936$ Å in composite-spectrum binaries, with specific reference to ζ Aurigae (K4 Ib + B5 V). The emission is detected in the isolated spectrum of the B-type dwarf secondary, and while $\lambda\,4102$ Å is heavily blended with Hδ, $\lambda\,3905$ Å falls in the B-star's featureless continuum. The narrowness of the emission ($v_{\mathrm{turb}} \simeq 6$ km s^{-1}) demonstrates that it originates in the upper photosphere or deep chromosphere of the K star primary. We propose that photoexcitation by the hot star's UV continuum, followed by recombination and cascades, leads to resonant scattering and subsequent pumping of lower opacity transitions in the singlet and triplet systems of Si I. This process channels the UV continuum into select narrow emission lines. We have also identified weaker photoexcited emission of Fe II at $\lambda\,3938.289$ Å. The strengths, positions, and widths of the $\lambda\,3905$ Å emission line vary with orbital phase owing to changes in the dilution of the irradiating flux and in the geometrical aspect of the irradiated hemisphere. Utilizing the inherent spatial resolution provided by the illuminated patch, and assuming that the K star is spherical with isotropic emission, yields $v\sin i \sim 5.7$ km s^{-1}. Evidence of tidal distortion was deduced from the timing of the rapidly rising phase of the emission just after periastron. Increasing the diagnostic potential requires radiative transfer modelling of the formation and centre-to-limb variation of the emission.

Key words: line: formation – binaries: eclipsing – binaries: spectroscopic – stars: individual: ζ Aur – stars: individual: 32 Cyg – stars: individual: HR 2030.

1 INTRODUCTION

A composite-spectrum binary is traditionally defined as a system consisting of a late-type giant or supergiant and an early-type companion; the ratio of their luminosities is such that the spectra of both components are visible and blended, in the blue and near UV. The ζ Aur binaries are a subset that undergo atmospheric eclipses, thereby yielding detailed information about the physical properties of the chromosphere of the cool evolved primary. Sequences of observations made during atmospheric eclipse can provide details of the supergiant's atmosphere at the level of the pressure scale-height. For a modern review, see Ake & Griffin (2015).

Because of the astrophysical insight that can be derived uniquely from those eclipse phases, observations of ζ Aur binaries cluster very heavily around eclipse dates. However, needing to investigate

ζ Aur (K4 Ib + B5 V; Griffin et al. 1990) well away from eclipse, REMG and R. F. Griffin obtained another high-resolution spectrogram when the secondary star was *in front* of the primary, and were intrigued to find a strong emission line at $\lambda\,3905$ Å. Subsequent examination of fairly low-dispersion archived Mount Wilson (MW) spectra of ζ Aur revealed a strong correlation between the emission strength of $\lambda\,3905$ Å and that of Ca II K.

When the secondary spectrum was isolated by subtracting the primary's spectrum, a technique described in detail by Griffin & Griffin (1986), another emission line was detected at $\lambda\,4102$ Å, just on the redward side of the core of Hδ. Its close proximity to Hδ (see Fig. 1, panel f) makes it difficult to detect even against the isolated secondary spectrum. Nevertheless, emission at $\lambda\,4102$ Å has definitely been observed in spectra of that region whenever the $\lambda\,3905$ Å line is bright. The two lines were identified as Si I $\lambda\,3905.523$ Å (RMT 3; Moore 1945) and Si I $\lambda\,4102.936$ Å (RMT 2). The laboratory wavelengths of the lines are known accurately, with $1\sigma_{\Delta v} \leq 0.1$ km s^{-1} (Radziemski & Andrew 1965; Kramida et al. 2014). We refer to them hereafter as $\lambda\,3905$ Å and $\lambda\,4102$ Å. A study of other

★E-mail: graham.harper@colorado.edu (GMH); elizabeth.griffin@nrc-cnrc.gc.ca (REMG); pbennett@ap.smu.ca (PDB)
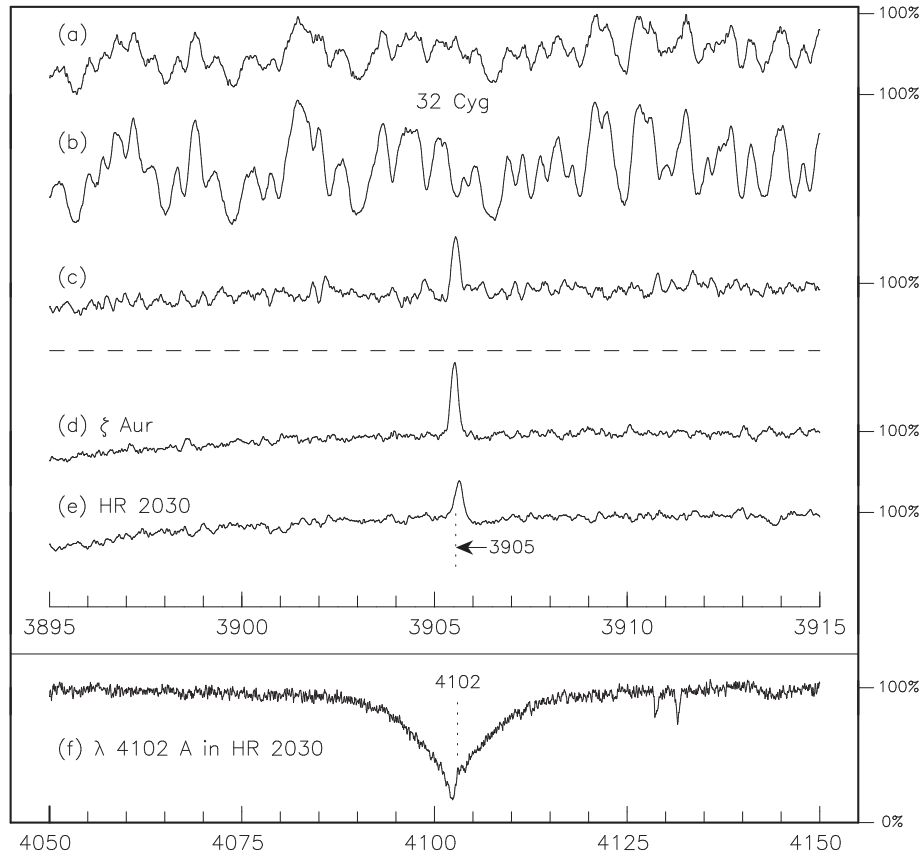
Figure 1. Si I in emission in composite-binary systems. In order to isolate the emission features it is necessary first to subtract the spectrum of the cool evolved star; the emission is then seen against the secondary's continuum. Panel (a) shows the composite spectrum of 32 Cyg A+B (K5 Ib + B6 V) in the region of λ 3905 Å; subtracting a suitable proportion of the spectrum of 32 Cyg A (seen during totality), shown in panel (b), uncovers the spectrum of 32 Cyg B, as seen in panel (c). Panels (d) and (e) show the same feature in ζ Aur and HR 2030, respectively. Data source: DAO spectra at 2.2 Å mm^{-1}. Panel (f), derived from MW photographic observations at 10 Å mm^{-1}, shows the uncovered spectrum of the hot secondary in HR 2030 in the region of Hδ. Emission at λ 4102 Å is certainly present, but cannot be measured accurately in any of these systems owing to heavy blending with Hδ. However, its appearance in emission simultaneously with that of λ 3905 Å provides a strong confirmation of the identity of the phenomenon. These examples illustrate the sharpness of the emission.

composite-binary systems revealed convincing occurrences of the same emission in the ζ Aur system 32 Cyg (K5 Ib + B6 V), and in the non-eclipsing system HR 2030 (K1 II + B8.5 V; Griffin & Griffin 2000). The recovery of emission at λ 3905 Å in 32 Cyg is illustrated in panels (a)–(c) of Fig. 1, which also shows examples of emission in λ 3905 Å in the isolated spectra of the B-type secondary stars of ζ Aur (d), HR 2030 (e). The emission lines are remarkably sharp; in ζ Aur a 1988 photographic high-resolution spectrum (2.2 Å mm^{-1}) shows a FWHM of 13 km s^{-1}, compared to 4.8 km s^{-1} for arc lines, and it is comparably narrow in 32 Cyg and HR 2030 (Fig. 1).

This detection of Si I emission in ζ Aur is in fact a re-discovery of the phenomenon first announced by Christie & Wilson (1935) in a footnote added 'while in press', where its actual discovery was attributed to W.S. Adams, who had noticed it on a plate taken in 1935 (phase .09).[1] Christie and Wilson mentioned that subsequent observations showed that the line 'has widened and increased in intensity' but that no other emission features were detected. They gave its measured wavelength as λ 3905.45 Å. No reference was made to λ 4102 Å, no doubt because of its close proximity to Hδ. At optimal phases the emission in ζ Aur is strong enough to be

detected visually in the composite spectrum, as was the case when Adams first noticed it. In the other two systems it is less strong even at maximum, and cannot be detected unambiguously unless the secondary spectra are fully isolated.

In a footnote which refers to the footnote in Christie & Wilson (1935), Walter (1937) reported that Si I λ 3905 Å was 'clearly'[2] [sic] detected in three ζ Aur spectra (his fig. 2) obtained in 1935 between phases .07 and .11. He also showed that, between phases .95 and .11, Ca II H & K in ζ Aur went from absorption to emission.

In this paper, we demonstrate that the source of the λ 3905 Å emission in ζ Aur is a result of B-star radiation illuminating the visible hemisphere of the K supergiant, as suggested by Christie & Wilson (1935), and we also develop a natural explanation for the observed emission strengths.

Fig. 2, a partial Grotrian diagram for Si I, shows how λ 3905 Å arises from a singlet $^1P_1$ upper level of Si I, whereas λ 4102 Å is an intercombination line arising from a triplet $^3P_1$ upper level and is intrinsically weaker. The relevant atomic data are presented in Table 1. The ground triplet term and the next two terms (singlets) have even parity and are expected to be populated with a Boltzmann distribution because collisions will dominate the weak radiative transitions

---

[1] All orbital phases in this paper are measured from periastron. Mid-eclipse occurs near phase .93.

[2] German: *deutlich*; in fact that description seems optimistic.
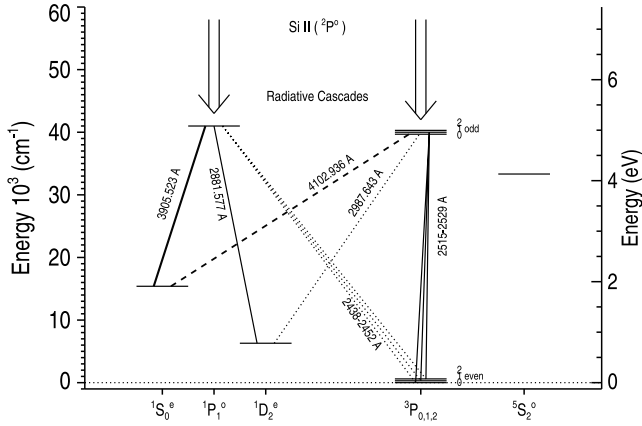
Figure 2. Partial Grotrian Diagram for Si I showing λ 3905 Å and λ 4102 Å and interconnected transitions. The lower terms are dominated by triplets and singlets.

between them. Radiative excitation of Si I is therefore expected to be dominated by absorption from these triplet and singlet systems, while the first odd quintet term will have a very low population in the K-star atmosphere: the quintet terms are weakly coupled to the Si II ground term and therefore have smaller photoionization and radiative recombination rates than do the triplet and singlet terms.

A potential complication to isolating the B-star spectrum from the composite one arises because the K-star spectrum obtained during eclipse may still contain contaminating signal. During total eclipse, some B-star photons are scattered back into the line of sight by the opacity in the extended K-star chromosphere and stellar wind (see Stencel et al. 1984). The sources of that opacity are predominantly strong lines from singly- and doubly-ionized species, though not from neutral species (which have very small ionization fractions) nor from intrinsically weak transitions (Eaton 1992). The extraction of Si I emission using the K-star eclipse spectrum should therefore be free from contamination from this scattering process, but it does have implications for other potential photoexcited features that arise from strong transitions of abundant species, e.g. Fe II, where the spectral subtraction procedure might lead to imperfect isolation of the feature.

The formation of λ 3905 Å and λ 4102 Å is an interplay between the phase (ϕ) varying system geometry, $\mathcal{G}(\phi)$, and the line formation, $\mathcal{L}$, through atomic physics and atmospheric structure, so the emission-line flux can be written symbolically as

$$\mathcal{F}(\phi) = \mathcal{G}(\phi) \times \mathcal{L} \times \mathcal{C}(\mathcal{G}, \mathcal{L}), \qquad (1)$$

where $\mathcal{C}(\mathcal{G}, \mathcal{L})$ is the coupling between geometry and line formation (e.g. limb darkening). We examine each term in turn in Sections 3 and 4, using as a test case our spectroscopic observations of ζ Aur, for which we have relatively precise orbital and physical parameters and thorough orbital coverage (illustrated in Fig. 3). A natural measure of these spectroscopically determined emission-line strengths is the emission equivalent width (EEW) as measured against the B-star spectrum.

Emission in Si I λ 3905 Å is not new to astrophysics, as it has been known to occur in long-period variables, e.g. Joy (1926), Merrill (1923), Willson (1976), though in parallel with other strong emission lines, mainly of H. Si I λ 3905 Å has also been observed in symbiotic stars (Merrill 1950), and during solar flares (Cauzzi et al. 1996).

This paper is organized as follows: observations of the emission are described in Section 2, and the properties of the λ 3905 Å line emission and centroid velocities are explored in Section 3. A photon-counting picture for the formation of λ 3905 Å and λ 4102 Å is presented in Section 4, while in Section 5 we interpret the results and discuss the potential of the emission as a unique diagnostic for stellar physics. Conclusions are presented in Section 6.
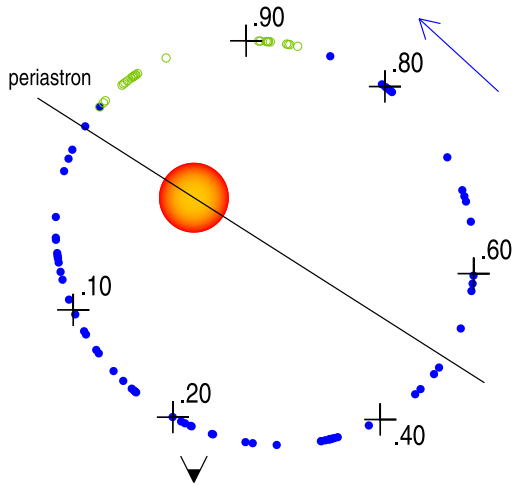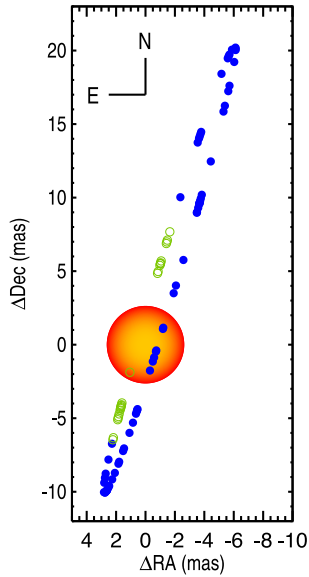
2 SPECTROSCOPIC DATA

2.1 Observations

Our data base of observations of the λ 3905 Å region includes over 100 high-dispersion spectra of ζ Aur, some historic lower dispersion observations, plus enough spectra of HR 2030 and 32 Cyg to provide supporting evidence. In about 25 per cent of the cases two, and occasionally more, observations were made consecutively, and could be co-added in order to improve the S/N ratio. The dates and measurements for the resulting 91 spectra of ζ Aur are listed in Table 2. Of those, 76 (embracing all since 2000) were recorded on a SITe-4 CCD with the 96-inch camera at the coudé focus of the Dominion Astrophysical Observatory (DAO) 1.2-m (48-inch) telescope, using the spectrograph in high-dispersion mode (2.2 Å mm^{-1}) at a resolving power of $R \sim 45\,000$ (Richardson 1968). The earlier spectra were recorded photographically, and include 10 with the MW 100-inch telescope and coudé spectrograph (nine were borrowed from the MW plate archive), and four with the Calar Alto (CA) 2.2-m telescope and coudé spectrograph (f/12 and f/3 systems). We also had access to a higher resolution CCD observation ($R \sim 65\,000$) taken with the Echelle Spectrograph on the Gunma Astronomical

Table 1. Si I atomic data for relevant bound–bound radiative transitions.

No.	Wavelength (Å)	Upper-level	Lower-level	Multiplet	$\mathrm{Log}_{10}(gf)$ (Smith et al. 1987)	$\mathrm{Log}_{10}(gf)$ (Garz 1973)
1	2452.118	$4s\,^1P_1^o$	$3p^2\,^3P_2$	UV 2	-2.74 ± 0.07	
2	2443.364	$4s\,^1P_1^o$	$3p^2\,^3P_1$	UV 2	-2.71 ± 0.07	
3	2438.768	$4s\,^1P_1^o$	$3p^2\,^3P_0$	UV 2	-2.61 ± 0.07	
4	2881.577	$4s\,^1P_1^o$	$3p^2\,^1D_2$	UV 43	-0.03 ± 0.07	-0.15 ± 0.06
5	3905.523	$4s\,^1P_1^o$	$3p^2\,^1S_0$	RMT 3	-0.98 ± 0.07	-1.09 ± 0.06
6	2514.316	$4s\,^3P_1^o$	$3p^2\,^3P_0$	UV 1	-0.79 ± 0.07	-0.76 ± 0.04
7	2519.202	$4s\,^3P_1^o$	$3p^2\,^3P_1$	UV 1	-0.92 ± 0.07	-0.89 ± 0.04
8	2528.508	$4s\,^3P_1^o$	$3p^2\,^3P_2$	UV 1	-0.70 ± 0.07	-0.66 ± 0.04
9	2987.643	$4s\,^3P_1^o$	$3p^2\,^1D_2$	RMT 1	-2.08 ± 0.14	-2.02 ± 0.06
10	4102.936	$4s\,^3P_1^o$	$3p^2\,^1S_0$	RMT 2	$< -2.59 \pm 0.13$	-3.14 ± 0.08

but they are heavily – in the latter case, exclusively – concentrated towards phases near and during total (primary) eclipse when the hot dwarf is occulted by the cool giant. That subset has no bearing on the present study, for reasons now understood (and explained below); Si I has never been detected in emission at phases close to, or during, primary eclipse.

2.2 Data extraction

The CA photographic spectra were observed at either 2.2 or 8.8 Å mm^{-1} and were calibrated in intensity with the aid of a portable auxiliary spectrograph, as described in detail by Griffin & Griffin (1979); the MW plates bore their own direct-intensity calibrations. The plates were digitized either with a modified Joyce–Loebl microdensitometer at the Institute of Astronomy (Cambridge, UK) or with the PDS scanner[4] of the former Royal Greenwich Observatory. Spectra from the high-dispersion exposures were extracted in steps of 10 mÅ, and from the lower dispersion ones in steps of 50 mÅ. The CCD spectra from the DAO were processed by a pipeline that incorporated standard IRAF routines.

The spectra were extracted in the rest-frame of the supergiant component by making use of the grating equation, as described by Griffin et al. (1990). In that procedure, the positions of identified stellar lines (determined by cross-correlating with a symmetrical profile) are assigned their laboratory wavelengths. Application of the grating equation to a set of positions then yields the rest-frame wavelength scale together with precise values of the parameters of the spectrograph. The composite spectra were therefore aligned in wavelength with that of the total eclipse, since in both cases the identified lines for the wavelength reduction were those of the cool supergiant. That procedure was critical for a correct performance of the subtraction procedure which was then applied to isolate the spectrum of the secondary component (ζ Aur B), as outlined by Griffin et al. (1990). For the great majority of the CCD spectra, the eclipse spectrum which we used in the subtraction process was that of JD 54927.67 (phase .943), observed on 2009 April 6, after mid-eclipse (the point is visible in Fig. 3).

Since λ 3905 Å was not present in the supergiant's spectrum (i.e. in total eclipse) that was used to remove the contribution of the primary from the composite ones, λ 3905 Å therefore showed up at relevant phases in the corresponding *secondary* spectra. ζ Aur B is of sufficiently early spectra type that it does not have any intrinsic spectral features at or near λ 3905 Å (see Fig. 1), so the continuum of each spectrum of the secondary star could be levelled quite precisely across a 10 Å stretch centred on the wavelength of the emission line. The spectra were also normalized to a continuum level of 100 per cent.

The equivalent width of the emission feature was measured by summing the recorded intensities, relative to the continuum, between specified wavelengths. Its central position was measured online by fitting manually a bisector at the half-maximum level; since the profiles were susceptible to small distortions by noise, any more sophisticated procedures would probably have returned less consistent measurements. The equivalent width of each observation is recorded in column 4 of Table 2. Radial velocities (column 5) were derived relative to the laboratory rest wavelength of λ 3905.523 Å. A dash indicates that no measurement could be made, mostly because the feature was not present, or (infrequently) because

Figure 3. Top: orbital sampling of our spectral coverage (circles) of ζ Aur shown on the plane of sky, relative to the K primary. The small circles describe the location of the B star corresponding to the observations listed in Table 2. Bottom: the spectral coverage is now shown in the plane of the orbit; selected phases indicated. The filled (blue) circles correspond to Si I λ 3905 Å detections, and the open (green) ones to non-detections. In both figures the orbit and K star are shown to scale.

Observatory (GAO) 1.5-m telescope in Japan;[3] the objective of the latter was to resolve the emission-line profile, but the observation was also used to measure the line strength. There is sufficient material in Table 2 to conduct an analysis of the Si I emission in ζ Aur in considerable detail; its occurrence in 32 Cyg and HR 2030 will be the topic of subsequent analyses. We should add that the MW and DAO plate archives contain large numbers of observations of ζ Aur,

---

[3] Kindly obtained and reduced for us by O. Hashimoto and S. Honda.

[4] The instrument, now obsolete, was known universally by the initials of its original manufacturer, *Photometric Data Systems*.

Table 2. Spectroscopic Observations of ζ Aur. The full table is available online.

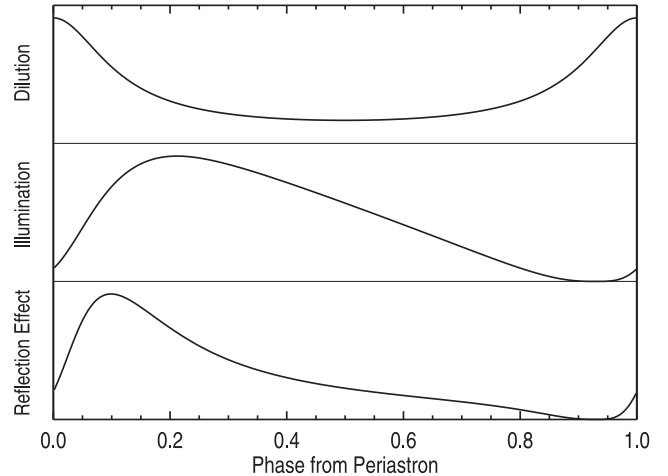| Spectrum ID	JD −2 400 000	ϕ	Si I EEW (mÅ)	Si I RV (km s^{-1})	Fe II EEW (mÅ)	Fe II RV (km s^{-1})
Ce 9396	35001.00	.445	48	–		
Ce 9491	35031.00	.476	32:	–	20	–
Ce 10305	35523.70	.983	–			
Ce 10341	35550.70	.011	59	−1.4	–	
Ce 10424	35584.70	.046	98	–		
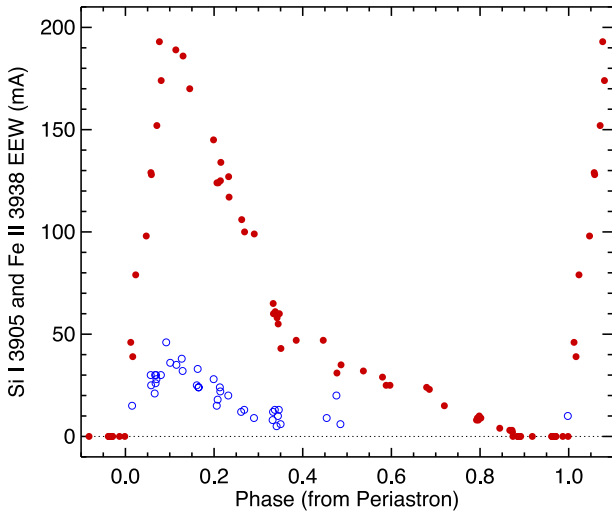
Figure 4. EEWs of Si I λ 3905 Å and Fe II λ 3938 Å as a function of orbital phase from periastron, using the orbit from Griffin (2005). The filled circles (red) depict λ 3905 Å; the empty circles (blue) depict λ 3938 Å and are a factor of ∼6 weaker. The rapid increase near phase .5 is a consequence of the substellar illumination coming into view round the limb of the supergiant.

Figure 5. The geometric contributions to the total reflection effect for ζ Aur as a function of phase from periastron. Top panel: variation in the geometric dilution factor due to the eccentricity of the orbit. Middle panel: the contribution from the illuminated K star visible from Earth. Bottom panel: the combined effect of the two above terms. It shows a remarkable similarity to the observed shape of the Si I EEW points shown in Fig. 4 (see Fig. 7).

it was weak and of inferior quality for a measurement to be meaningful.

A small emission feature near λ 3938.3 Å is also unquestionably present in the secondary spectra when the Si I one is easily visible, though being somewhat weaker than the latter it requires good S/N for precise measurement. We identified it as a member of Fe II RMT 3 (Moore 1945). Other, intrinsically fainter, members of the multiplet can be detected in the same spectra when 3938 Å is strong; two of those members (λ 3969.40 Å and λ 3969.38 Å) are mutually enhanced by close blending, but unfortunately they occur in the core of the Ca II H line at λ 3968.47 Å. The upper level of these Fe II lines is in the first odd-parity term (z ^{6}D^o), while the lower level is in the fourth even-parity term (a ^{4}P^e). This term arrangement is similar to that for the Si I λ 3905 Å and λ 4102 Å lines. Measurements of each EEW, made where possible, for the 3938 Å line are shown in column 6 of Table 2. Measurements of the positions of those lines were converted into radial velocities (column 7) by referring to the laboratory wavelength; National Institute of Standards and Technology (NIST) Atomic Spectra Data base (Kramida et al. 2014) quotes an observed value of λ 3938.289 Å, but we applied a correction of +0.010 Å in order to remove a small systematic displacement between the Si I and Fe II points. (Note: the NIST Ritz wavelength is given as 3938.294 Å.)

The EEWs for both λ 3905 Å and λ 3938 Å are illustrated in Fig. 4; the latter are about six times weaker than Si I and consequently somewhat noisier. Both lines show a similar shape as a function of phase, which indicates that (a) they are excited by the B star, and (b) both are formed near the K-supergiant photosphere.

3 ORBITAL VARIATION OF EEWS AND CENTROID VELOCITIES: $\mathcal{G}(\phi)$

In this section, we describe the properties of the two Si I emission lines as a function of orbital phase, measured from periastron. First we examine the phase variation shown in Fig. 4, and establish that the excitation source is illumination by the B-star's UV continuum. We then discuss emission-line profile velocity constraints, which reveal that the emission originates in the photosphere or deep chromosphere.

3.1 EEW Characteristics of λ 3905 Å

Fig. 5 illustrates the classic Eddington reflection effect as a function of phase calculated following Eddington (1926) and Sobolev (1975).[5] The close similarity to the shape of the EEW data in Fig. 4 is clear. The reflection effect is composed of two geometric terms; the first is the fraction of the visible K star that is illuminated by the B star, and the second is the varying dilution of that radiation resulting from the changing separation of the stars around the eccentric orbit. The close agreement in shape is further evidence that the emission in λ 3905 Å and λ 4102 Å originates in the atmosphere of the K supergiant.

---

[5] We follow the practice of referring to the line re-emission as a *reflection effect* even though the process is actually that of *amplification*.

Table 3. Orbital and stellar parameters used in the PHOEBE model light curve.

Eccentricity	0.3930 ± 0.0023	Griffin (2005)
Systemic velocity	$+12.11 \pm 0.04$ km s^{-1}	ditto
Period	972.164 ± 0.041 d	ditto
ω	$327.5 \pm 0°\!\!.4$	ditto
Periastron passage†	MJD 47204.8 ± 0.9	ditto
i	$87.0 \pm 1°\!\!.3$	Bennett et al. (1996)
Mass		
$\quad$ ζ Aur A	5.8 ± 0.2 M$_\odot$	ditto
$\quad$ ζ Aur B	4.8 ± 0.2 M$_\odot$	ditto
Radius		
$\quad$ ζ Aur A	148.0 ± 3 R$_\odot$	ditto
$\quad$ ζ Aur B	4.5 ± 0.5 R$_\odot$	ditto
$T_{\rm eff}$		
$\quad$ ζ Aur A	3960 ± 100 R$_\odot$	ditto
$\quad$ ζ Aur B	15200 ± 200 R$_\odot$	ditto

† Conjunction occurs at .929.

The possibility that the $\lambda\,3905$ Å emission is caused by scattering in the line can be eliminated quantitatively. When the substellar point is centred on the visible hemisphere of the K-star, the relative flux increase from reflection is (from Eddington 1926)

$$\mathcal{G}(\alpha) = \frac{\Delta F}{F} \simeq \frac{2}{3}\left[\sin^2\phi_0 + \left(2 + \cos^3\phi_0 - 3\cos\phi_0\right)/\sin\phi_0\right]$$

$$\sim \frac{2}{3}\left(\frac{R_K}{d}\right)^2, \tag{2}$$

where $\sin\phi_o$ is the ratio of the K-star radius to the separation of the two components; $\sin\phi_o = R_K/d$. For ζ Aur, $d \sim 6R_K$, giving a flux increase of the order of 2 per cent – an order of magnitude smaller than is observed.

The emission in $\lambda\,3905$ Å and $\lambda\,4102$ Å must therefore be due to a line-formation mechanism which channels the radiative energy effectively into specific wavelengths. We posit that the irradiation by the hot star causes photoexcitation, including photoionization, leading to subsequent radiative recombination and cascades. The emission should have the same phase variation as reflection, as it depends on the separation of the components, and on the amount of the visible K-star hemisphere that is being illuminated. The radiative time-scales for scattering and recombination are expected to be short compared to orbital time-scales, so the emission will track the substellar point (see Section 4.1).

In order to examine that phase variation in detail, we constructed a model of the ζ Aur system with the binary light-curve code PHOEBE (Degroote et al. 2013) that takes account of the reflection effect and – importantly – any tidal distortion of the K star. The parameters of the model are given in Table 3; the velocity orbital elements are from Griffin (2005). The light curve was also compared to one generated from the orbital elements of Eaton, Henry & Odell (2008); they differ by <0.1 per cent. The light curve was found to be insensitive to the degree of synchronicity between the stellar and orbital rotation of the K-star.

The K-star illumination at selected phases is shown in Fig. 6, while the light curve and the data are reproduced in Fig. 7. That close similarity between the reflection phase dependence and the Si I EEWs shows that the observed variation of the emission can be explained in terms of the geometry of the system. There are no significant systematic phase shifts from the observations, as would be the case if, for example, the 'hotspot' responsible for the Si emission lagged appreciably behind the substellar point. The ellipsoidal variation of the PHOEBE K-star model provides an improved match to the rapid rise in Si I emission, i.e. immediately after periastron, as compared to a fit with the spherical-star approximation of classical Eddington reflection; the ellipsoidal variations produce a phase shift of +.015. The sensitivity of the phases of the rapid EEW rise to the binary system parameters is given in Table 4.

While there is a good overall fit to the shape of the measured EEWs, there are two discrepancies visible in Fig. 7. First, the model
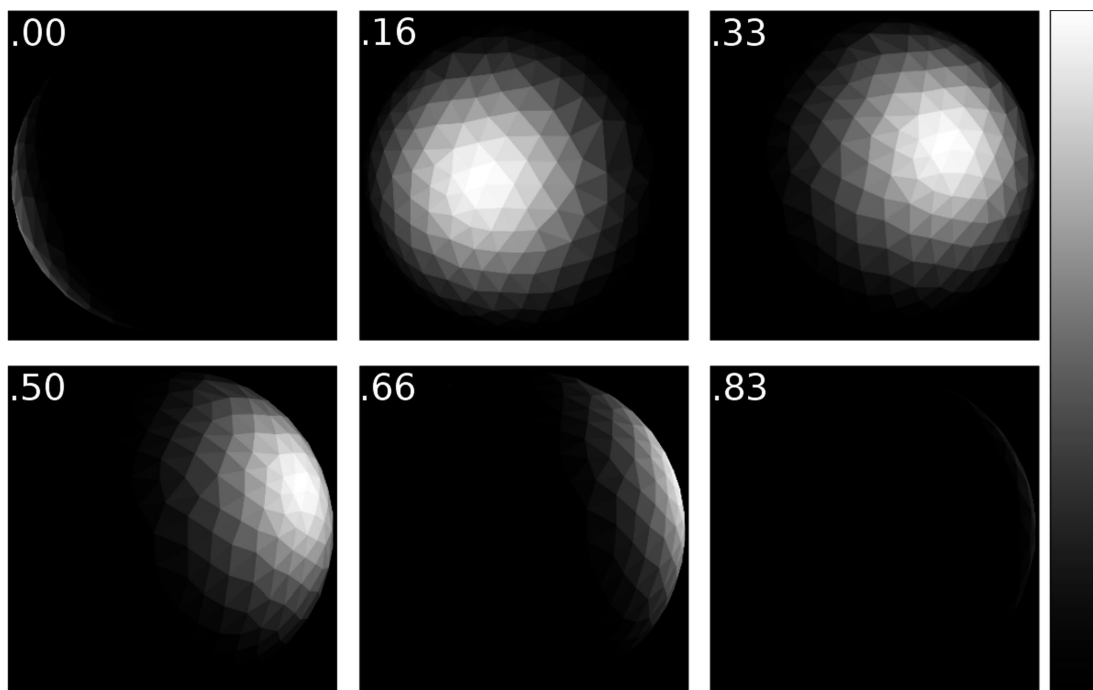
Figure 6. Six images representing the surface of the K star and the reflected B-star flux, as calculated using PHOEBE. They show (from top left to bottom right) phases .00, .16, .50, .66, and .83, respectively (measured from periastron).

Table 4. Sensitivity of the phase of rapid emission rise to system uncertainties.

Parameter	Order of change in phase variation of reflection curve
Orbital parameters:	
Bennett et al. (1996) – Griffin (2005)	$\sim$0.1 per cent
K star Radius:	
$147\,R_\odot$ (Bennett et al. 1996) – $160\,R_\odot$ (Schröder et al. 1990)	$\sim$0.1 per cent
Stellar masses:	
$M_B = 4.8 \pm 0.2\,M_\odot$ & $M_K = 5.8 \pm 0.2\,M_\odot$ (Bennett et al. 1996)	$\sim$0.1 per cent
Synchronicity parameter:	
$P_{rot} = C P_{orb}$ $C = [0, 1]$	$\sim$1 per cent
Gravity darkening parameter:	Does not alter the phase variation
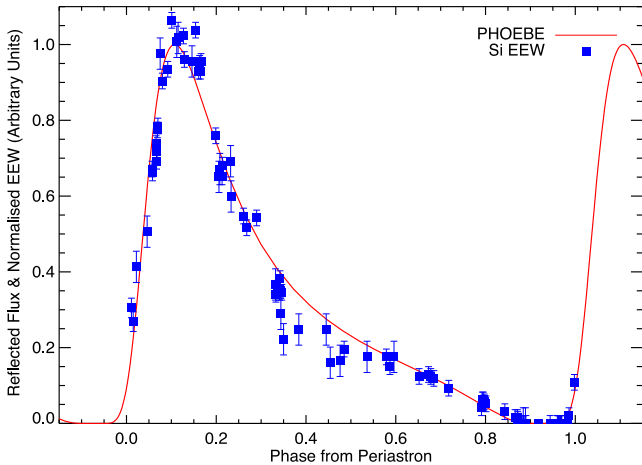
Figure 7. Reflected light curve, calculated using PHOEBE, fitted to the Si I EEWs; we have assigned a coarse error estimate to the observations. The vertical scale was derived by a least-squares fit to all the data.

underpredicts the emission near its peak at phase .10, and second, between phases .35 and .55, the model overpredicts the strengths of the observations. Since the data were collected over a number of different orbits, three possible explanations suggest themselves: (1) the description of the K-star geometry is not complete, (2) the angle-dependent re-emission from the K star leads to a phase-dependent modification, or (3) the heating of the K-star chromosphere and upper photosphere by the B star has induced changes to its structure sufficient to modify the interpretation of the Si I EEWs obtained by spectrum subtraction. These options are discussed in Section 4.

3.2 Velocities: line widths

Although the primary purpose of the observing programme was to measure the strength of the emission line, we could also derive some velocity constraints. The measured FWHM are $\simeq 0.17\,\text{Å}$ (13 km s^{-1}), which are of the order of the resolution of the CCD spectra, but this is significantly broader than the intrinsic resolution of the high-resolution photographic and the GAO $R \sim 65\,000$ spectra, implying that the line is resolved in the latter two cases. In addition, we note that (a) absorption lines formed in the K-star wind are $\sim$50 km s^{-1} wide, (b) the $\lambda\,3905\,\text{Å}$ wind opacity is expected to be totally negligible, (c) lines formed in the B-star photosphere have widths $v\sin i \simeq 200$ km s^{-1} (Bennett, Brown & Linsky 1995), and (d) velocities of 13 km s^{-1} or below are only expected to be found in the low chromosphere or photosphere of the K supergiant.

A width of 13 km s^{-1} is comparable to the non-thermal micro-turbulence, v_{mic}, that was derived from optical spectra near first contact. Values for the tangential microturbulence (*most probable velocity*) have been given as 7–9 km s^{-1} (Wilson & Abt 1954), or 15 km s^{-1} (Schröder, Griffin & Griffin 1990); however, since the gas and magnetic Reynold's numbers are expected to be very large (Dorch 2004), the chromosphere might be highly turbulent. In that case the magnitude of the radial turbulence might be similar to the tangential motions.

We analysed the GAO spectrum (phase .154), by subtracting an appropriate eclipse spectrum, noting that the disc-integrated K-star eclipse spectrum is rotationally broadened and therefore intrinsically smoother than the emission line. The measured FWHM of the GAO observation of $\lambda\,3905\,\text{Å}$ was is 12.3 km s^{-1}, which corresponds to a deconvolved *most probable* radial turbulent velocity of 6 km s^{-1} (after a small correction for rotational broadening). The result strongly suggests that the emission is formed in the upper photosphere or deep chromosphere. The photospheric microturbulence is 2.3 km s^{-1} (Wilson & Abt 1954), while our value of 6 km s^{-1} is similar to, or slightly smaller than, the values of photospheric radial-tangential macroturbulence found in K Ib stars by Gray & Toner (1987).

3.3 Line shifts

In Fig. 8 we plot the emission-centroid shifts as a function of phase, thereby providing information about the projected velocity of the upper photosphere/deep chromosphere, and whether the K-star's rotation is synchronized (or pseudo-synchronized) with the orbit.

If we assume *Lambertian* (isotropic) emission from a spherical K star, we find a best fit of $v\sin i \simeq 5.7$ km s^{-1}. The scatter is larger than expected from wavelength and measurement uncertainties, and the measured velocities are sensitive to the combined systematic errors introduced by the subtraction process, so we cannot assign a formal uncertainty. The inclusion of limb-brightening/darkening in the model of the Si I emission is expected to lead to systematic offsets of the order of 1 km s^{-1}; the value of $v\sin i$ may be refined at a later time.

An indirect disc-integrated estimate for $v\sin i$ of 6.8 ± 1 km s^{-1} was obtained by de Medeiros & Mayor (1999) with the Haute-Provence *Coravel*; it includes an empirical correction for luminosity-dependent non-rotational broadening mechanisms. The Cambridge *Coravel* value of 8.4 km s^{-1} given by Griffin (2005) has not been corrected for sources of non-rotational broadening, so the two are consistent. Including the angular dependence of the emission will refine the derived $v\sin i$, as also will the inclusion of some geometric distortion of the K star. The result from our model is
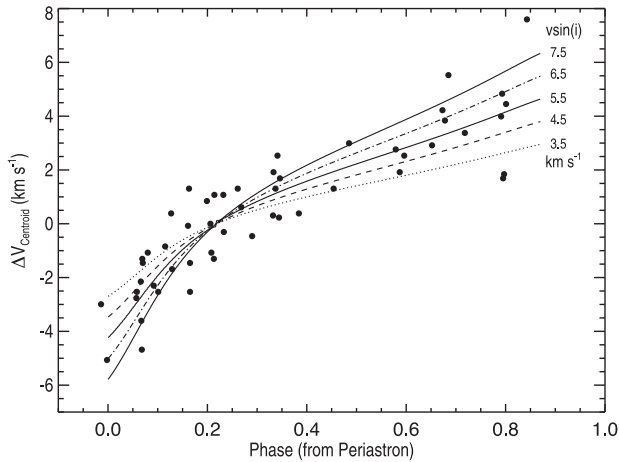
Figure 8. Velocity shifts of the Si I λ 3905 Å line-centroid as a function of phase from periastron, in the rest frame of the K star. Model fits for different $v \sin i$ are shown for a spherical star when isotropic emission is assumed. The best fit here is with $v \sin i = 5.7$ km s^{-1}, but experimentation with limb-darkened/brightened emission suggests a systematic uncertainty of ~1 km s^{-1} can be expected.

substantially larger than the value suggested by Eaton et al. (2008), whose argument (based on disc-integrated absorption-line depths) concluded that ζ Aur might have $v \sin i$ of 2.5 km s^{-1}. Our higher value is in fact consistent with the 7 km s^{-1} or so found for K Ib stars by Gray & Toner (1987), de Medeiros & Mayor (1999), and De Medeiros et al. (2002). It is of interest to see if our direct estimate of $v \sin i$ corresponds to orbital synchronization or pseudo-synchronization (i.e. the rotational velocity at periastron). Eaton et al. (2008) predicted $v \sin i = 8.3$ km s^{-1} for synchronization, and 16.6 km s^{-1} for pseudo-synchronization, using expressions in Hut (1981). In agreement with the conclusion of Eaton et al. (2008), our Si I $v \sin i$ value excludes pseudo-synchronization. Because intermediate-mass K Ib stars typically have $v \sin i$ of that magnitude, it may not be possible to establish from observations whether orbital synchronization of the rotational velocity has or has not occurred.

Griffin et al. (1990) measured the projected velocity of the chromosphere observed at the limb during the 1987 eclipse, finding a value of 8.5 ± 0.14 km s^{-1} from observations made on Nov 16, citing an impact parameter of 163 R$_\odot$; when scaled to the stellar radius of 148 R$_\odot$ (Bennett et al. 1996) for solid-body rotation, this corresponds to a photospheric value of 7.7 km s^{-1}. Future high-resolution observations combined with radiative transfer modelling of the intensity–angle relation for Si I λ 3905 Å should enable the $v \sin i$ for this system to be resolved, and more detailed information about the intrinsic and chromospheric rotational velocities to be extracted.

4 Si I 3905 Å: LINE FORMATION, $\mathcal{L}$

In this section, we consider the atmospheric conditions expected in the λ 3905 Å line-forming region, and apply them to identify the important formation processes in order to guide our predictions of EEW strengths.

The observed fluxes from the two component stars are comparable near λ 4100 Å, but at the surface of the K star the geometric dilution of the B-star radiation is such that the fluxes are equal near λ 3000 Å. Radiation shortward of this may lead to differences in the illuminated and unilluminated K-star atmosphere. The UV absorp-
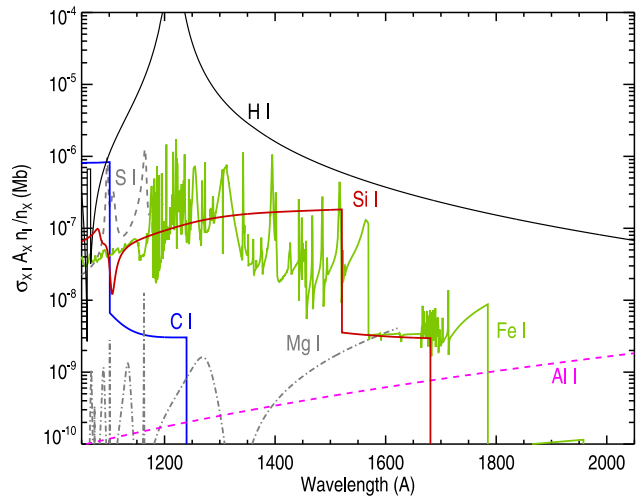
Figure 9. Photoionization cross-sections for neutral species, weighted by abundance and the estimated ionization fraction. The strong edges of Si I and Fe I are clearly visible longward of H Ly α. Although H Rayleigh scattering only has a small cross-section, coherent scattering is seen to play an important role in reducing the amount of B-star radiation in the deep chromosphere/upper photosphere when the abundance and ionization balance of the neutral species is factored in. Electrons ejected from photoionization thermalize in the chromosphere, while coherent scattering conserves photons.

tion opacity is dominated by neutral bound–free edges (see Fig. 9); most abundant singly ionized species have their ground-state cross-sections at shorter wavelengths, in the H Lyman continuum.

The B-star radiation which falls upon the K-star's outer atmosphere will eventually interact with an atom, ion, or molecule. Previous studies have shown that the B-star's UV radiation can photoionize atoms which have low first-ionization potentials (low-FIP) more readily than can the K star's intrinsic radiation field. However, because of the great depth of formation of λ 3905 Å in the atmosphere, the short-wavelength component of the far-UV will be Rayleigh-scattered by K-star neutral hydrogen. Some photons will scatter back into space and some will diffuse inwards, effectively forming a short-wavelength cut-off to the B-star's ionizing flux.

4.1 Conditions within ζ Aur A's lower chromosphere

Over the past 50 yr there have been a number of studies of the chromospheric structure of ζ Aurigae systems: see Griffin et al. (1990, and references therein), Eaton (1993), and Wright (1970). To study the line formation of λ 3905 Å and λ 4102 Å we first consider estimates of the gas temperature, T_{gas} (which will be equal to the electron temperature, T_e), the hydrogen density (n_H) and column density (N_H), and electron density (n_e) taken from the literature.

Studies of partial-eclipse ingress phases, i.e. those with the smallest impact parameter, have been presented for 1939 Dec 19 by Wilson & Abt (1954), and for 1987 Nov 17 by Schröder et al. (1990). Wilson & Abt found a Boltzmann excitation temperature, T_{exc}, of 3500–4500 K, and curve-of-growth tangential turbulence velocities of 6–8 km s^{-1} (slightly larger than we deduced from the λ 3905 Å emission profile), while Schröder et al. found the somewhat higher values of 12–16 km s^{-1} and $T_{exc} \simeq 5000$ K. At these projected heights, $n_H \sim 2 \times 10^{11}$ cm^{-3} and $N_H \sim 6 \times 10^{22}$ cm^{-2}. Low-FIP metals are observed to be singly ionized, e.g. $n_{Fe\,I}/n_{Fe\,II} \sim 5 \times 10^{-4}$, $n_{Mg\,I}/n_{Mg\,II} \sim 1 \times 10^{-3}$, $n_{C\,I}/n_{C\,II} \sim 2 \times 10^{-4}$, and $n_{S\,I}/n_{S\,II} \sim 6 \times 10^{-4}$ (Schröder et al. 1990; Eaton 1993). Balancing

photoionization and recombination rates gives $n_e \sim 10^9 \, \text{cm}^{-3}$, implying that hydrogen is the principal electron donor since $n_e/n_H \simeq 5 \times 10^{-3}$, a value that is higher than can be supplied by low-FIP metals on their own (Schröder et al. 1990; Eaton 1993). Since no estimates appear to have been derived for the Si ionization balance, we scaled the more reliable Fe I/Fe II ratio by the ratio of the estimated photoionization rates; both systems have similar recombination rates at those temperatures (Nahar 1995; Nahar, Bautista & Pradhan 1997). We therefore adopted $n_{\text{Si I}}/n_{\text{Si II}} \simeq 8 \times 10^{-5}$.

The optical depth of the Si I photoionization edge is given by $\tau_{b-f} = \sigma_{\text{edge}} A_{\text{Si}} N_H n_{\text{Si I}}/n_{\text{Si II}}$, where A_{Si} is the Si abundance relative to hydrogen (here we adopt $A_{\text{Si}} = 3.5 \times 10^{-5}$), and $\sigma_{\text{edge}} \simeq 65$ Mb is the photoionization cross-section at the edge. Adopting the above values from the partial-eclipse studies yields $\tau_{b-f} \simeq 0.01$, but we know that the bulk of the B-star's UV radiation must be absorbed where $\tau_{b-f} \geq 1$, closer to the photosphere. The intrinsically narrow widths of the emission lines also indicate that they probably form closer to the photosphere than the partial-eclipse chromosphere.

To estimate conditions deeper in, we can take advantage of the property that the chromospheric heating in ζ Aur, as judged from the intrinsic K-star emission observed in low-opacity lines during the eclipse of the B star, is similar to that of other similar single, evolved stars (Schröder et al. 1988; Eaton 1993; Harper et al. 2005). The semi-empirical chromospheric model of the eclipsing system 22 Vul (G5: Ib:+ B8 V; Griffin et al. 1993) has a temperature minimum, $T_{\text{min}} = 3550$ K, with a hydrogen column density $N_H \simeq 4 \times 10^{24} \, \text{cm}^{-1}$ (Marshall 1996), while in the case of the single K4 II bright giant α TrA, $N_H \simeq 10^{24} \, \text{cm}^{-1}$ (Harper 1992). The chromospheric thickness scaling law of Ayres (1979) suggests that the chromospheric conditions for ζ Aur will be similar: the derived values of n_H and $n_e/n_H \simeq 5 \times 10^{-3}$ are indeed similar to those of α TrA at $T_e = 5000$ K, again suggesting that the deepest layers probed during chromospheric eclipse are farther out than ζ Aur K-star's temperature minimum.

Selecting thermodynamic properties that are characteristic of a higher N_H, so as to ensure $\tau_{b-f} \geq 1$, we adopt $T_e = T_{\text{min}} \simeq 0.75 \, T_{\text{eff}} \simeq 3000$ K, $n_H = 10^{14} \, \text{cm}^{-3}$, $n_e/n_H = 2 \times 10^{-4}$, $N_H = 3 \times 10^{24} \, \text{cm}^{-2}$.

Fig. 9 shows the continuum opacity contributions derived by assuming solar abundances except for C, which has a reduced abundance of $A_C = 2.2 \times 10^{-4}$, as is typical of evolved intermediate-mass stars that have undergone the first dredge-up (Luck & Lambert 1985). The effective cross-sections include the abundances and the ionization fractions described above. At these depths, scattering by neutral hydrogen becomes an important opacity source longward of Ly α. We have adopted the analytic H Rayleigh scattering cross-sections given by Gavrila (1967). Under the conditions near the temperature minimum, the hydrogen optical depth approaches unity near $\lambda 1450$ Å. We took the bound–free photoionization cross-sections for Si I from Nahar & Pradhan (1995), for Fe I from Bautista (1997), for Mg I from Mendoza & Zeippen (1987), and for C I from Nahar & Pradhan (1997), with additional data from the compilation of cross-sections by Mathisen (1984, and references therein). For S I, we adopted the photoionization cross-sections from the Opacity Project data base TOPBASE (Cunto et al. 1993), which were fitted as needed with Henry, Lorentz or Fano profiles (Fano 1961; Fano & Cooper 1965).

4.2 Bound–bound or bound–free excitation?

Rather than solving the full complex radiative transfer problem (non-local thermodynamic equilibrium, multi-ion,

multiwavelength) with its own inherent uncertainties, we constructed instead a simple photon-counting model in order to explain (a) why the emission is predominantly present in Si, (b) the relative strength of $\lambda 3905$ Å and $\lambda 4102$ Å, (c) the absence/weakness of other Si I emission lines, and (d) the strengths of the analogous C I lines at $\lambda 2478.561$ and 2582.898 Å. In Section 5 we discuss the formation of the newly discovered weak emission in Fe II $\lambda 3938$ Å.

Excitation of Si I can occur by exciting both the bound–bound (line) and the bound–free (continuum) transitions. For bound–bound transitions, once a B-star photon has been absorbed from the populated low excitation levels (singlets and triplets of even parity), the excited Si I electron can either return to its original state or cascade down through the dominant singlet and triplet terms. After photoionization, the Si II will recombine via radiative recombination, because dielectronic recombination only becomes important for electron temperatures $T_e \geq 10^4$ K (Nahar & Pradhan 1995). It will preferentially recombine to the singlet and triplet systems because the Si I quintet system does not couple strongly to the Si II ground state.

To estimate the fraction of UV photons which interact with Si I bound–bound and bound–free opacity, we constructed a simple model for the K-star's opacity that considered the first two ionization states of the first 28 elements. The energy levels were restricted to those terms that are adjacent to, and have the same parity as, the ground term. Collisional interactions with electrons and hydrogen should ensure that those levels have populations close to a Boltzmann distribution. The line-list was based on a compilation of semi-empirical oscillator strengths for transitions between observed energy levels (Kurucz & Bell 1995). For the adopted T_e, turbulence broadening and ionization balances, we computed the fraction of the total opacity at each wavelength that resulted from Si I.

The B-star's radiation field was computed from a detailed photospheric model of the B star generated with TLUSTY (Hubeny 1988). We adopted the effective temperature and surface gravity for ζ Aur B reported by Bennett et al. (1995), *viz.* $T_{\text{eff}} = 15200$ K, $\log_{10} g_*(\text{cm s}^{-2}) = 3.82$, and computed a synthetic spectrum from the B-star photospheric model using SYNSPEC, described by Hubeny & Lanz (2011) and Hubeny, Stefl & Harmanec (1985).

For Si I, we found that bound–bound transitions make up ~ 20 per cent of total Si I interactions with the UV radiation field. These simple estimates suggest that radiative recombination dominates the excitation of $\lambda 3905$ Å and $\lambda 4102$ Å. In our photon-counting model we now consider just the competing bound–free absorption. Fig. 10 illustrates the spectral region where the B-star's radiation incident on the K star photoexcites the Si I system, and shows the estimated attenuation of the B-star's spectrum by Rayleigh scattering. Only a fraction of the far-UV photons absorbed by Si I is eventually emitted at $\lambda 3905$ Å. To calculate the EEW, we computed the following expression:

$$\text{EEW} \propto \left(\frac{hc}{\lambda_{3905}} \right) \frac{1}{F_{3905}} \int_{912}^{1986} F_\lambda \frac{\lambda}{hc} \frac{\kappa_\lambda^{\text{Si I}}}{\kappa_\lambda^{\text{tot}}} d\lambda. \tag{3}$$

F_λ is the B star flux, and κ is the bound–free absorption cross-section. The integral represents the number of B-star photons absorbed by Si I in the far-UV; the lower and upper wavelength limits are the Lyman continuum and the Si I $^1S_0^e$ bound–free edge, respectively. The leading term represents the inverse of the number of photons in 1 Å of the B-star's continuum at 3905 Å. In practice, the effective lower wavelength limit to the integral is larger, owing to the decline of the (attenuated) B-star's continuum and to absorption by C I and S I. Evaluating equation (3) at a single representative
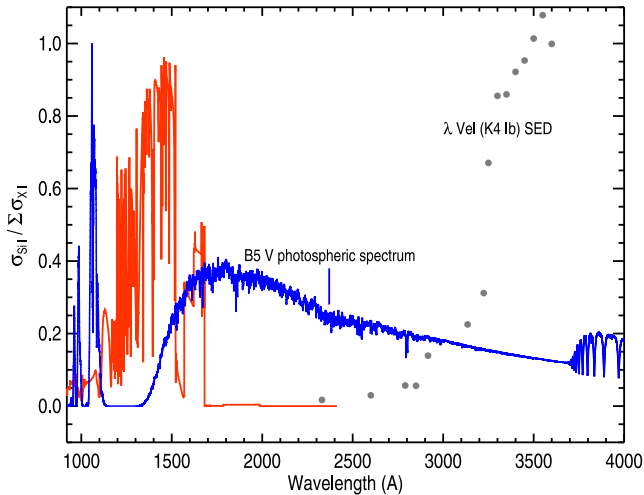
Figure 10. The ratio of bound–free opacity from Si I to total bound–free opacity, for the conditions described in the text. Also included is an estimate of the shape of the scaled B-star's spectrum attenuated by H Rayleigh scattering near the line-forming region, where we have assumed that half of the photons are scattered forwards. A fraction of the photons absorbed into the Si system is eventually emitted at λ 3905 Å and λ 4102 Å, and seen superimposed on the B-star spectrum after the K star contribution has been removed from the composite spectrum. The grey/filled circles indicate the surface spectral energy distribution of the spectral-type proxy (λ Vel, K4 Ib) plotted on the same scale as the B star. The λ Vel data were taken from Carpenter et al. (1999) and Kiehling (1987).

depth gives a value of ∼70, but we still have to account for geometric factors and for the efficiency of formation of λ 3905 Å. The main uncertainties in our result are the attenuation of the B-star radiation field, and relative ionization balances and cross-sections; the latter uncertainty is of the order of 10–100 per cent. Because of the simplifications built into the photon-counting model, we cannot expect the overall precision to be any better than of the order of unity.

4.3 Calculating the λ 3905 Å formation efficiency ($\mathcal{L}$)

Next we investigate the fraction of the Si photoexcitation that leads to emission in λ 3905 Å and λ 4102 Å. To zeroth-order, the number of radiative recombinations into Si I can be approximated by the statistical weighting factors for the singlet and triplet systems, i.e. 1/4 (singlet) and 3/4 (triplet). *R*-matrix calculations of state-specific radiative recombination rates suggest that 19 per cent of the top 74 per cent of the total recombination rates at $T_e = 3000$ K go into singlet terms (Nahar 2000). Recombination into singlet terms will lead preferentially to cascades within that system. Here, we assume that 0.19 of the total recombinations (singlet plus triplet) eventually populate the upper level of the λ 3905 Å transition, and that 0.81/3 of the recombinations into the triplet system eventually populate the upper level ($J = 1$) of the λ 4102 Å transition.

The ratio of line to bound–free opacity for Si I can be written as

$$\frac{\tau_{b-b}}{\tau_{b-f}} \simeq 4\lambda gf \frac{n_l}{n_{\mathrm{ground}}}, \qquad (4)$$

where gf is the weighted oscillator strength (Table 1), λ is the wavelength in Å, and n_l/n_{tot} is the fractional population of level l (see Table 5). An optical depth of unity for the λ 1521 Å edge gives line-centre optical depths (τ_0) of 150 for λ 2881 Å and 0.3 for λ 3905 Å. As can be deduced from the Grotrian diagram in Fig. 2,

Table 5. Energy Levels[a] of Si I corresponding to Fig. 2, and their Boltzmann populations at two representative temperatures.

Level	Energy (cm^{-1})	J	Designation	Boltzmann population ($T_{\mathrm{exc}} = 3000$)	Boltzmann population ($T_{\mathrm{exc}} = 4000$)
1	0.000	0	3p^2 ^{3}P	1.2×10^{-1}	1.1×10^{-1}
2	77.112	1	3p^2 ^{3}P	3.4×10^{-1}	3.2×10^{-1}
3	223.157	2	3p^2 ^{3}P	5.2×10^{-1}	5.1×10^{-1}
4	6298.847	2	3p^2 ^{1}D	2.8×10^{-2}	5.7×10^{-2}
5	15394.362	0	3p^2 ^{1}S	7.2×10^{-5}	4.3×10^{-4}
6	33326.040	2	3p^2 ^{5}S^o	6.6×10^{-5}	3.4×10^{-6}
7	39683.158	0	4s ^{3}P^o		
8	39760.285	1	4s ^{3}P^o		
9	39955.051	2	4s ^{3}P^o		
10	40991.888	1	4s ^{1}P^o		

[a] Martin & Zalubas (1983)
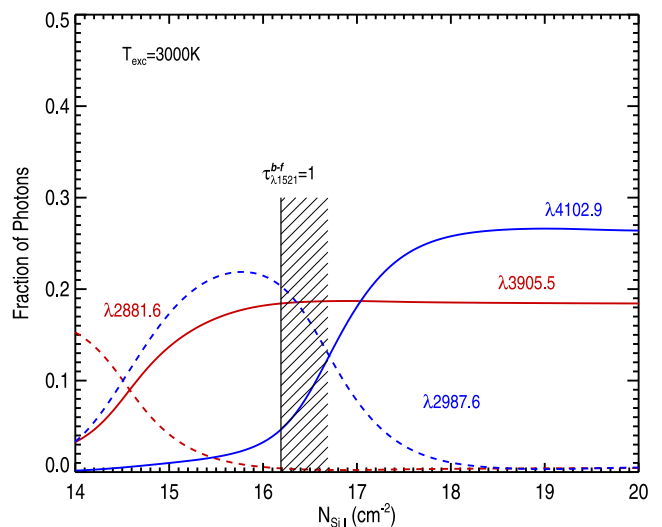
Figure 11. Fraction of photons emitted in λ 4102 Å, λ 3905 Å, and the two UV lines. We have assumed that the terms adjacent to, and of the same parity as, the ground term (see Fig. 2) are populated by a Boltzmann distribution at $T_e = 3000$ K. The peak in the radiative recombination is predicted to occur near the shaded region, where the ground-term bound–free edge has an optical depth $\tau \geq 1$.

photons in the opaque λ 2881 Å line undergo multiple scattering, resulting in enhanced emission in the lower opacity λ 3905 Å line (see Jordan 1967). That is consistent with the observation that the line is narrow and not opacity broadened.

4.3.1 Escape probability model

The degree of λ 3905 Å pumping, just described, can be evaluated via escape probability theory, by computing the relative number of photons emitted for the transitions listed in Table 1. We evaluated the Doppler line profile K_2 function using the description by Hummer (1981); see also Rybicki (1984). We adopted a photospheric microturbulence of 2.3 km s^{-1} from Wilson & Abt (1954).

Fig. 11 shows the fraction of photons emitted in certain lines for a model atom whose lower same-parity levels are assumed to be populated by a Boltzmann distribution and in which the upper levels are not quenched by collisions. λ 3905 Å and λ 2881 Å are both strong lines, and the reduced probability of escape for λ 2881 Å effectively enhances the emission at λ 3905 Å. The ratio

of the $\lambda\,3905\,\text{Å}$ to $\lambda\,4102\,\text{Å}$ emission strengths is predicted here to be $\simeq 4$. Unfortunately the strength of $\lambda\,4102\,\text{Å}$ is difficult to measure owing to severe blending with Hδ in the B-star spectrum, but for JD 47431.63 an EEW of 54 mÅ was measured, suggesting a ratio of ~ 2.4. Adopting a slightly larger gf value for $\lambda\,4102\,\text{Å}$, e.g. from Smith et al. (1987) rather than Garz (1973), would improve the agreement with observation; on the other hand, we have neglected collisional coupling within the $^3P^e$ term, which might be important if we have underestimated the densities in the line-forming region. At this point, therefore, we cannot use the ratio of the EEWs to constrain the current model further, but it is not inconsistent. Fig. 11 shows that $\lambda\,2987.6\,\text{Å}$ is also an efficient escape route; its profile should be detectable with the *HST* high-resolution UV Space Telescope Imaging Spectrograph (STIS).

Combining the line-formation efficiency derived above with the fraction of photons absorbed by Si I, and the orbitally modulated geometric dilution term gives our model for Si I $\lambda\,3905\,\text{Å}$ EEW phase variation. This photon counting picture yields a phase curve that is only a factor of 1.4 larger than observed, which is relatively good agreement but is fortuitous since the calculation of the $\lambda\,3905\,\text{Å}$ yield included two terms with expected accuracies of order unity (even though the geometric term was tightly constrained). There is an ample supply of B-star UV photons to drive the $\lambda\,3905\,\text{Å}$ and $\lambda\,4102\,\text{Å}$ emission, and the overall agreement between the calculated curve and the measured EEWs suggests strongly that the essentials of the line-formation mechanism have been correctly identified.

4.4 C I $\lambda\,2478.561$ and $2582.898\,\text{Å}$

C I is abundant, and has the same term structure as Si I for the lower terms. We therefore explored the detectability of C I $\lambda\,2478.561\,\text{Å}$ and $2582.898\,\text{Å}$, which are the counterparts of $\lambda\,3905\,\text{Å}$ and $\lambda\,4102\,\text{Å}$. The first consideration is that the C I ground and photoionization edges from same-parity terms are at $1101\,\text{Å}$ ($2p^2\,^3P$), $1240\,\text{Å}$ ($2p^2\,^1D$), and $1445\,\text{Å}$ ($2p^2\,^1S$). They are significantly shortward of those for Si I; however, shortward of Ly α there is some cancellation of contributions to the Rayleigh-scattering cross-section, resulting in an overall reduction in attenuation. At $T_e = 3000$ K the C I ground term is dominant, and our photoionization model suggest that C I will absorb about half of the photons compared to the amount absorbed in Si I. We have examined archived *IUE* high-resolution spectra, but the inferior signal to noise and lower spectral resolution compared to our optical Si I data prevent positive detection of emission in the C I lines. It would be useful to search for them at appropriate phases with STIS.

4.5 Coupling between geometry and line formation, $\mathcal{C}\,(\mathcal{G}, \mathcal{L})$

In this paper we have considered only the major terms in the line-formation problem, and have disregarded any weak coupling represented by the correlation term ($\mathcal{C}$) between the phase-dependent geometry and the line-formation process. We do not anticipate that the supergiant's non-spherical geometry or recombination time-lags will change the formation efficiency: the recombination time-scale for Si II, $\tau_{rec} \simeq 5 \times 10^{11}/n_e$ (cm^{-3} s^1), is of the order of a few minutes and is therefore much too rapid, in relation to the differential motion between the substellar point and a given location on the K-star's surface, to give rise to any significant effects. The escape probability model suggests that when the B-star radiation is not incident along the line of centres then there will be more attenuation

from Rayleigh scattering, and also a reduced radial optical depth in the $\lambda\,2881\,\text{Å}$ line. Evaluation of these more subtle effects requires additional detailed modelling.

5 RESULTS AND DISCUSSION

The full phase dependence of the $\lambda\,3905\,\text{Å}$ emission shows that the source of the excitation is radiation from the B star, as suggested by Christie & Wilson (1935). The emission as a function of phase closely follows the Eddington reflection effect for a spherical K star with isotropic scattering, and is controlled by two terms: the separation of the two stars, which governs the amount of B-star flux that is intercepted, and the fraction of the photoexcited substellar illumination that is visible from Earth. Introducing geometric distortion of the K star by using PHOEBE improves the agreement between theory and observation for ζ Aur for the phases when the EEW is increasing rapidly. However, there are some recurring differences in the shape of the EEW curve between phases .35 and .55 that are revealed by virtue of the abundance of observations covering many cycles of the orbit. The highest resolution spectrum (from GAO) provided a value of $v_{turb} = 6$ km s^{-1}, indicating that the emission is formed in the deep chromosphere/upper photosphere. Our measurements of the centroid shifts of $\lambda\,3905\,\text{Å}$, corresponding to different regions of the substellar illumination on the visible K-star hemisphere, provided a direct determination of $v\sin i = 5.7$ km s^{-1} (for a spherical, isotropic model), a value that is typical of its spectral type (De Medeiros et al. 2002).

The photon-counting model presented here predicts EEWs that are sufficiently close to those observed as to lend full confidence to our general interpretation of the line formation. A full radiative solution to the problem is beyond the scope of this paper, but it would return detailed angle-dependent variations of the emission, leading to a more refined EEW phase curve and an improved direct measurement of $v\sin i$. One could then probe the origins of the EEW shape with greater confidence, particularly with respect to the degree of geometric distortion.

Irradiated chromospheres provide a testbed for investigating the structure and heating of cool stellar atmospheres. *HST* K-star eclipse spectra show that ζ Aur A's chromospheric heating and velocity fields are typical of single stars with similar spectral-types, e.g. λ Vel (K4 Ib; Carpenter et al. 1999; Harper et al. 2005), thus supporting a broader applicability of such a study. The illuminating B-star radiation field is well characterized through a combination of direct observations and synthetic photospheric spectra, and given recent improvements in atomic data, including photoionization cross-sections of neutral species, other photoexcitation processes may also be examined.

Irradiation provides a source of atmospheric heating of the K star, which may change its chromospheric structure and potentially affect the formation of $\lambda\,3905\,\text{Å}$ and $\lambda\,4102\,\text{Å}$. The K-star's intrinsic chromospheric heating is balanced predominantly by Ly α, Mg II h & k, Ca II H & K, and Fe II cooling, and is estimated to be $F_* \sim 3 \times 10^5$ erg cm^{-2} s^{-1}, based on λ Vel. Following Judge & Stencel (1991) we assumed that Mg II h & k account for $\simeq$ 25 per cent of the total losses, which Pérez Martínez, Schröder & Cuntz (2011) give as $\simeq 10^5$ erg cm^{-2} s^{-1}. The total unattenuated B-star flux incident on the K supergiant is $\sim 7 \times 10^7$ erg cm^{-2} s^{-1}, or 0.5 per cent of the K-star photospheric flux. Potentially there is sufficient flux available to modify the *irradiated* chromosphere and this may explain the excitation of Ca II H & K, first reported by Walter (1937) and confirmed here. CO, which exists in the lower chromospheres of cool evolved stars (Wiedemann et al. 1994), might be

photodissociated by line absorption shortward of λ 1100 Å, which would change the atmospheric energy balance and lead to an increase in local gas temperature. Research into this aspect of the problem would be fruitful.

The weak Fe ii lines discovered in our spectra are probably not formed by recombination from Fe iii. There is not expected to be much flux at the photoionization edges of Fe ii, shortward of the Lyman continuum, within the K star chromosphere where hydrogen is mostly neutral. Since most of the abundant metals are singly ionized, it is possible that UV bound–bound photoexcitation may dominate photoionization. λ 3938 Å is an intercombination line that originates from $^6D^o$, the lowest term of opposite parity to the metastable ground terms. This term arrangement is also true for λ 4102 Å. For λ 3938 Å, therefore, the excitation could be from the photoexcitation of bound–bound transitions followed by cascades down to the upper term whose transitions to the ground $^6D^e$ term are optically thick and pump the lower optical depth λ 3938 Å line whose lower level is $^4P^o$. The close similarity between the shapes of the Fe ii phase curve and that for Si i indicates that the Fe ii emission also forms close to the K-star photosphere, and not in an extended wind flow. Exploration of other wavelength regions, especially in the UV, may reveal other photoexcited emission lines.

6 CONCLUSIONS

Measurements of a large sample of extracted spectra of the λ 3905 Å region in the composite-spectrum binary ζ Aur, together with a detailed quantitative investigation into the physical and geometrical conditions that cause the periodic Si i λ 3905 Å emission phenomenon, have enabled us to understand the basic line-formation processes. The study has indicated how the emission-line profile can be used as a diagnostic for stellar rotation and surface velocity fields. Accurate measurements of the wavelengths of the emission line offer a new method to (a) obtain spectroscopically the rotation of the K supergiant, by tracking the substellar patch across the illuminated hemisphere during that section of its orbit, and (b) constrain the supergiant's atmospheric velocity fields in well-defined atmospheric layers.

The effects of irradiation on the K-star atmosphere by an accurately characterized B-star spectrum provide an opportunity to test our understanding of stellar atmospheric structure, especially the response to a change in chromospheric ionization balance and additional heating. Detailed radiative transfer modelling is now required to refine the interpretation of these observations, and to hone our understanding of the processes involved. A future study of the analogous C i lines observed with STIS on *HST* could provide additional valuable constraints.

REFERENCES

Ake T. B., Griffin E., 2015, Giants of Eclipse: The ζ Aurigae Stars and Other Binary Systems. Springer-Verlag, Berlin
Ayres T. R., 1979, ApJ, 228, 509
Bautista M. A., 1997, A&AS, 122, 167
Bennett P. D., Brown A., Linsky J. L., 1995, ApJ, 455, 317
Bennett P. D., Harper G. M., Brown A., Hummel C. A., 1996, ApJ, 471, 454
Carpenter K. G., Robinson R. D., Harper G. M., Bennett P. D., Brown A., Mullan D. J., 1999, ApJ, 521, 382
Cauzzi G., Falchi A., Falciani R., Smaldone L. A., 1996, A&A, 306, 625
Christie W. H., Wilson O. C., 1935, ApJ, 81, 426
de Medeiros J. R., Mayor M., 1999, A&AS, 139, 433
De Medeiros J. R., Udry S., Burki G., Mayor M., 2002, A&A, 395, 97
Degroote P., Conroy K., Hambleton K., Bloemen S., Pablo H., Giammarco J., Prša A., 2013, in Pavlovski K., Tkachenko A., Torres G., eds, EAS Publ. Ser. Vol. 64, Setting a New Standard in the Analysis of Binary Stars, p. 277
Dorch S. B. F., 2004, A&A, 423, 1101
Eaton J. A., 1992, MNRAS, 258, 473
Eaton J. A., 1993, ApJ, 404, 305
Eaton J. A., Henry G. W., Odell A. P., 2008, ApJ, 679, 1490
Eddington A. S., 1926, MNRAS, 86, 320
Fano U., 1961, Phys. Rev., 124, 1866
Fano U., Cooper J. W., 1965, Phys. Rev., 137, A1364
Garz T., 1973, A&A, 26, 471
Gavrila M., 1967, Phys. Rev., 163, 147
Gray D. F., Toner C. G., 1987, ApJ, 322, 360
Griffin R. F., 2005, Observatory, 125, 1
Griffin R., Griffin R., 1979, A Photometric Atlas of the Spectrum of Procyon λλ3140-7470 Å. The Observatories, Cambridge
Griffin R., Griffin R., 1986, JA&A, 7, 195
Griffin R. E. M., Griffin R. F., 2000, MNRAS, 319, 1094
Griffin R. E. M., Griffin R. F., Schröder K.-P., Reimers D., 1990, A&A, 234, 284
Griffin R. E. M., Hunsch M., Marshall K. P., Griffin R. F., Schröder K. P., 1993, A&A, 274, 225
Harper G. M., 1992, MNRAS, 256, 37
Harper G. M., Brown A., Bennett P. D., Baade R., Walder R., Hummel C. A., 2005, AJ, 129, 1018
Hubeny I., 1988, Comput. Phys. Commun., 52, 103
Hubeny I., Lanz T., 2011, Astrophysics Source Code Library, record ascl:1109.022
Hubeny I., Stefl S., Harmanec P., 1985, Bull. Astron. Inst. Czech., 36, 214
Hummer D. G., 1981, J. Quant. Spectrosc. Radiat. Transfer, 26, 187
Hut P., 1981, A&A, 99, 126
Jordan C., 1967, Sol. Phys., 2, 441
Joy A. H., 1926, ApJ, 63, 281
Judge P. G., Stencel R. E., 1991, ApJ, 371, 357

Kiehling R., 1987, A&AS, 69, 465

Kramida A., Ralchenko Y., Reader J., NIST ASD Team, 2014. NIST Atomic Spectra Database (ver. 5.2), [Online]. Available at: http://physics.nist.gov/asd [2015, July 20]. National Institute of Standards and Technology, Gaithersburg, MD

Kurucz R., Bell B., 1995, Atomic Line Data (R.L. Kurucz and B. Bell) Kurucz CD-ROM No. 23. Mass: Smithsonian Astrophysical Observatory, Cambridge

Luck R. E., Lambert D. L., 1985, ApJ, 298, 782

Marshall K. P., 1996, MNRAS, 280, 977

Martin W. C., Zalubas R., 1983, J. Phys. Chem. Ref. Data, 12, 323

Mathisen R., 1984, Photo Cross-sections for Stellar Atmosphere calculations - Compilation of references and Data, Institute of Theoretical Astrophysics, University of Oslo, Publication Series 1

Mendoza C., Zeippen C. J., 1987, A&A, 179, 346

Merrill P. W., 1923, ApJ, 58, 195

Merrill P. W., 1950, ApJ, 111, 484

Moore C. E., 1945, Contrib. Princeton Univ. Obs., 20, 1

Nahar S. N., 1995, ApJs, 101, 423

Nahar S. N., 2000, ApJS, 126, 537

Nahar S. N., Pradhan A. K., 1995, ApJ, 447, 966

Nahar S. N., Pradhan A. K., 1997, ApJS, 111, 339

Nahar S. N., Bautista M. A., Pradhan A. K., 1997, ApJ, 479, 497

Pérez Martínez M. I., Schröder K.-P., Cuntz M., 2011, MNRAS, 414, 418

Radziemski L. J., Jr, Andrew K. L., 1965, J. Opt. Soc. Am., 55, 474

Richardson E. H., 1968, J. R. Astron. Soc. Can., 62, 313

Rybicki G. B., 1984, in Kalkofen W., ed., Methods of Radiative Transfer. Cambridge Univ. Press, Cambridge and New York, p. 21

Schröder K.-P., Reimers D., Carpenter K. G., Brown A., 1988, A&A, 202, 136

Schröder K.-P., Griffin R. E. M., Griffin R. F., 1990, A&A, 234, 299

Smith P. L., Huber M. C. E., Tozzi G. P., Griesinger H. E., Cardon B. L., Lombardi G. G., 1987, ApJ, 322, 573

Sobolev V. V., 1975, Light Scattering in Planetary Atmospheres. Pergamon Press, New York

Stencel R. E., Hopkins J. L., Hagen W., Fried R., Schmidtke P. C., Kondo Y., Chapman R. D., 1984, ApJ, 281, 751

Walter K., 1937, Z. Astrophys., 14, 62

Wiedemann G., Ayres T. R., Jennings D. E., Saar S. H., 1994, ApJ, 423, 806

Willson L. A., 1976, ApJ, 205, 172

Wilson O. C., Abt H. A., 1954, ApJS, 1, 1

Wright K. O., 1970, Vistas Astron., 12, 147

SUPPORTING INFORMATION

Additional Supporting Information may be found in the online version of this article:

Table 2. Spectroscopic Observations of ζ Aur. (http://mnras.oxfordjournals.org/lookup/suppl/doi:10.1093/mnras/stv2668/-/DC1).

Please note: Oxford University Press is not responsible for the content or functionality of any supporting materials supplied by the authors. Any queries (other than missing material) should be directed to the corresponding author for the article.

This paper has been typeset from a TEX/LATEX file prepared by the author.